# Numerical analysis of constitutive coefficients effects on FE simulation of the 2D orthogonal cutting process: application to the Ti6Al4V

M. Yaich[1,2] · Y. Ayed[1] · Z. Bouaziz[2] · G. Germain[1]

**Abstract** In this paper, a deep study of constitutive parameters definition effect is done in order to guarantee sufficient reliability of the finite element machining modeling. The case of a particular biphasic titanium alloy Ti6Al4V known by its low machinability is investigated. The Johnson-Cook (JC) elasto-thermo-visco-plastic-damage model combined with the energy-based ductile fracture criteria is used. Segmentation frequency, chip curvature radius, shear band spacing, chip serration sensitivity and intensity, accumulated plastic strain in the formed chip segments, and cutting forces levels are determined where their dependency to every constitutive coefficient is examined and highlighted. It is demonstrated from the separate variation of every plastic and damage parameters that an interesting finite element modeling (FEM) relevance is reached with the adjustment of JC strain hardening coefficients term, thermal softening parameter, exponent fracture factor, and damage evolution energy. Moderate and high cutting speeds are applied to the cutting tool in the aim to test their impact on shear localization, chip segmentation, and numerical forces levels as well as to approve previous highlighted findings related to constitutive parameters definition. In general, this study focuses on a prominent decrease in identification process cost with the previous knowledge of the most affecting constitutive coefficients while keeping an interesting agreement between numerical and experimental results.

**Abbreviations**

| | |
|---|---|
| JC | Johnson-Cook |
| ASB | Adiabatic shear band |
| FEM | Finite elements modeling |
| FEA | Finite elements analysis |
| $A$ | Initial yield stress (MPa) |
| $B$ | Hardening modulus |
| $n$ | Work hardening exponent |
| $C$ | Strain rate sensitivity coefficient |
| $m$ | Thermal softening coefficient |
| $T_{\mathrm{Ref}}$ | Reference temperature (°K) |
| $T_{\mathrm{melt}}$ | Melt temperature (°K) |
| $\overline{\varepsilon_{\mathrm{p}}}$ | Equivalent plastic strain |
| $\overline{\dot{\varepsilon}_0}$ | Reference plastic strain rate |
| $\overline{\dot{\varepsilon}_{\mathrm{p}}}$ | Actualized plastic strain rate |
| $\Delta\overline{\varepsilon}$ | Increment of updated plastic strain |
| $D_1$ | Initial failure strain |
| $D_2$ | Exponent factor |
| $D_3$ | Triaxiality factor |
| $D_4$ | Strain rate factor |
| $D_5$ | Temperature factor |
| $D$ | Johnson-Cook actualized state variable |
| $D_{ev.L}$ | Linear damage evolution |
| $D_{ev.Exp}$ | Exponential damage evolution |
| $L$ | Characteristic mesh element length (mm) |
| $u_f$ | Equivalent plastic displacement in totally fractured material |

| $u_p$ | Equivalent plastic displacement |
|---|---|
| $G_{f(I\ II)}$ | Fracture energy corresponding to tensile/shear mode (Nm$_{-1}$) |
| $k_c$ | Fracture toughness (MPa $\sqrt{m}$) |
| $E$ | Young modulus (GPa) |
| $\nu$ | Poisson's ratio |
| $\sigma_h$ | Hydrostatic stress (MPa) |
| $\sigma_{VM}$ | Von Misses stress (MPa) |
| $\sigma_y$ | Yield stress of machined material |
| $\sigma^*$ | Stress triaxiality (MPa) |
| $\tilde{\sigma}$ | Unreal stress state (when no damage is present) |
| $\mu$ | Coulomb's friction coefficient |
| $m_{\text{Tresca}}$ | Tresca factor |
| $k$ | Shear flow stress (MPa) |
| $\sigma_n$ | Normal stress (MPa) |
| $\tau_f$ | Friction stress (MPa) |
| $\eta_{p(f)}$ | Fraction of energy produced by material plastic (friction) work |
| $f_f$ | Fraction of heat transmitted to the cutting tool |
| $\dot{q}_{f(p)}$ | Heat flux created by material friction (plastic) work (Wm$^{-2}$) |
| $\dot{q}_{\rightarrow\text{Tool}}$ | Heat flow going to the cutting tool (Wm$^{-2}$) |
| $a_p$ | Depth of cut (mm) |
| $f$ | Feed rate (mm/rev) |
| $V_c$ | Cutting speed (m/min) |
| $F_c$ | Tangential force |
| $F_f$ | Feed force |
| $f_{\text{seg}}$ | Segmentation frequency |
| $R_c$ | Chip curvature radius (mm) |
| $L_s$ | Shear band spacing (mm) |
| $H$ and $h$ | Peak and valley chip thickness ($\mu$m) |
| $G_{\text{seg}}\%$ | Chip segmentation degree |
| $S_{\text{seg}}\%$ | Chip serration sensitivity factor |
| $\Delta\varepsilon_{p(\text{in-out})}$ | Accumulated plastic strain in a segment |
| CSI | Chip serration intensity |

# 1 Introduction

Machining process presents nowadays one of the most useful manufacturing methods which allow having a finished product with superior surface quality. Most of mechanical components, especially for those in titanium alloys, are produced with machining operation. This latter generally involves coupled thermomechanical conditions added to the high non-linearity caused by the interesting levels of strain, strain rate, and temperature undergone by the machined material. Therefore, the total understanding of the cutting process is still until now a great challenge that cannot be yet solved analytically or experimentally [1]. Interaction between different aspects like strain hardening, viscosity, thermal softening, hardening softening, loading history, and material microstructure changes that take place in extremely thin zone during a very short time period, as well as availability of many new and powerful software, are the origins of the wide use of finite element modeling (FEM) in these last decades. This method presents an irreplaceable tool in material machining modeling as well as in local and instantaneous information capturing. Hence, it allows a deep comprehension of several dynamic phenomena accompanying the cutting process and of course a best management of the contact conditions produced between the cutting tool and the workpiece. In fact, the use of the numerical method greatly helps in reducing from machining cost while ameliorating from the comprehension of machining phenomena [2]. Recently, finite element analysis (FEA) has been increasingly used instead of the analytical methods to focus on the different aspects of materials machining and to ameliorate its global control including the chip formation procedure [3], the cutting forces prediction [4], the temperature determination [4], the finished surface quality increase [5], and the tool wear prevention [6].

Produced chip resulted from machining operations can be qualitatively classified on four distinct categories (continuous, wavy, serrated, and discontinuous) depending on model geometry (rake and flank angles, chamfer length and angle, tool edge radius), cutting conditions (cutting speed, depth of the cut, feed rate), material properties (thermomechanical properties, failure initiation), and contact conditions. In fact, reproducing with enough precision the chip morphology is crucial since this latter presents a significant indicator about the whole cutting process stability and it deeply helps in well understanding and improving from machined surface integrity. In their study, Davies et al. [7] have concluded that the onset of whatever chip morphology strongly modify from the reached levels in terms of temperatures, cutting forces, tool wear evolution, and machined surface quality. Therefore, well mastering the cutting process is based on the accurate prediction of the chip formation mechanisms as well as of its specific characteristics.

In this investigation, machining modeling of a particular titanium alloy, the Ti6Al4V, is studied. This material, known by its interesting strength to density ratio, has been used in a variety of mechanical components subjected to severe operating conditions like corrosion, mechanical chocks, and high temperatures. However, the most drawback of this material is its low thermal conductivity combined with its high chemical reactivity with the cutting tool generally resulting on its accelerated wear [8]. In addition to its poor machinability, the dry machining of such difficult to cut metal is characterized by the frequent formation of a serrated chip even under low cutting conditions which is not the case of other materials [9]. This chip segmentation presents one of the most investigated phenomena that need to be accurately understood. Saw-toothed removed material results as reported in [10] on a high frequency of cutting forces oscillations as well as on an

interesting fluctuation in the cutting tool-workpiece contact length, which further accelerates the cutting tool wear thus reduces from the machined surface quality. These recent decades, many investigations have been done in order to accurately insight the major factors controlling the chip segmentation. In literature review, two theories about chip serration are generally found where the onset of such morphology has been attributed either to adiabatic shear bands (ASBs) theory [8, 11, 12] or to crack initiation and propagation [13–15].

Shaw and Vyas [14] have studied the case of high-strength steels machining. They have concluded that segmented even fragmented chip is respectively the result of partial or total crack propagation within the primary shear zone depending on the applied cutting conditions. The authors have concluded a particular damage propagation sense which starts from the free chip surface and disseminates to its interior side in contact with the cutting tool tip. Lin and Lin [15] have asserted, when modeling the 3D orthogonal cutting process of the 6-4 brass, the same origin of chip segmentation but with opposite sense of damage propagation. They have signaled that material failure initially appears in the bottom chip side just above the cutting tool edge and progressively propagates along the chip thickness until achieving its free surface.

Contrariwise, other studies have explained chip segmentation phenomenon by the thermoplastic shear instability produced within the chip thickness. This instability is mainly produced when the thermal softening effect becomes more pronounced than the strain hardening one. High strains produced in narrow regions of the machined material leads to its softening because of the heat rise concentration within. In this regard, Ambati and Yuan [12] have suggested that ASBs formation presents the most significant phenomena responsible of the chip segmentation where softened material is characterized by its high susceptibility to be plastically deformed due to its mechanical characteristics drop that contributes to a partial upward motion of the removed material above the formed band.

In fact, whatever the chip segmentation origin (ASB formation, fracture initiation and propagation, or even the combination between them), the FE model is requested to perfectly reproduce material separation process, shear stresses localization, and chip segmentation in the case of machining modeling. It is also asked to simulate plastic strain increase and temperature rise in the removed material coupled with its strength drop in order to accurately predict cutting forces, temperature levels, and residual stresses distribution. That is why in the last decades, many efforts have been done in the aim to increase the effectiveness of numerical models in reproducing the cutting process. However, FEM has demonstrated the particular attention that should be attached not only to the accurate implementation of numerical parameters (such temporal integration, formulation type, mesh density) but also to the right definition of material constitutive models which

are asked to perfectly describe the elasto-thermo-visco-plastic-damage behavior of the machined material.

A diversity of constitutive models has been developed and used by many authors in the case of machining modeling. This diversity is mainly due to the coupled effects taken into account and the number of the coefficients that need to be identified. Meanwhile, the use of one material constitutive law and not the others could be justified by how much of reliability might be cheeked through the definition of one specific model. Nonetheless, achieving interesting accuracy of FEM remains until now a great challenge that needs to be overcome. Effectively, in order to guarantee much correlation with experimental results, it is important when determining constitutive parameters and for whatever the flow stress expression to reproduce as same as possible the encountered severe loading conditions accompanying the metal cutting process and especially for the Ti6Al4V. In this case, extremely high strains are involved, causing an interesting strain rate and temperature rise within the machined material (in the range of $10^2$– $10^6$ s$^{-1}$ and up to 1000 °C, respectively).

The Johnson-Cook (JC) constitutive law [16] appears very interesting to be used in metal machining simulation since it allows the coupling between different effects (hardening, strain hardening, and thermal softening) with a minimum number of coefficients (only five). Its common use in many investigations of hard machining modeling is explained also by its implementation in different FE commercial softwares. Additionally, the wide availability of JC parameters values in literature review corresponding to a variety of materials encourages its growing use. However, the possibility of finding more than one JC parameter sets determined for the same material (see Table 1) presents one of this model drawback that cannot be ignored since it strongly influences on prediction quality in terms of material flow description, chip morphology, cutting forces, and temperature distribution once they are not suitably selected. This distinction is essentially due to the different thermal heat treatments applied to the machined material as well as to the adopted method used in parameters identification.

Since this distinction in constitutive coefficients heavily affects numerical model accuracy, precision in JC coefficients identification is still focused in the aim to achieve interesting correlation between numerical and experimental results. Literature review illustrates that JC constants have been identified experimentally and/or numerically. Even if the first method is frequently used, its principal limitation is that the tested conditions are extremely far from those really reached in cutting operations. Strain and strain rate levels achieved in simple tensile, compression, or shear tests are much lower than those encountered in the machining tests (up to 0.5 and $10^3$ s$^{-1}$, respectively) [9, 19]. The inability of these experimental tests to reproduce important loading conditions similar to those encountered during real cutting tests recommends usually

**Table 1** Different JC constants values of the Ti6Al4V

| References<br>Designation | | [8]<br>JC-a | [9]<br>JC-b | [17]<br>JC-c | [9]<br>JC-d | [18]<br>JC-e | [17]<br>JC-f |
|---|---|---|---|---|---|---|---|
| Initial yield stress (MPa) | $A$ | 782.7 | 870 | 884 | 968 | 983 | 1119 |
| Hardening modulus (MPa) | $B$ | 498.4 | 990 | 599 | 380 | 348 | 838.6 |
| Work hardening exponent | $n$ | 0.28 | 0.25 | 0.362 | 0.421 | 0.32 | 0.473 |
| Strain rate dependency coefficient (MPa) | $C$ | 0.028 | 0.011 | 0.034 | 0.0197 | 0.024 | 0.019 |
| Thermal softening coefficient | $m$ | 1 | 1 | 1.04 | 0.577 | 0.69 | 0.643 |
| Initial strain rate (s$^{-1}$) | $\dot{\varepsilon}_0$ | – | – | 1 | 0.1 | 0.1 | 1 |

the extrapolation of the flow stress curves preceding the final determination of the constitutive parameters as reported by Chen and al [20]. Even if this fitting step is randomly done, it helps however in overcoming the quite difference between the statement stress states in specimen and the induced ones in simulated machined workpiece. In fact, constitutive coefficients validity should be questioned outside those experimental tested ranges since the flow stress extrapolation cannot take into account the actualized behavior of the machined material. Another problem generally encountered with experimental identification even if high strain rates tests are performed (thanks to Gleeble simulator use) is how to guarantee the same material treatment for both the specimen and the machined workpiece. Nonetheless, experimental methods usually suffer from cost because of the need to acquisition posts treatment with high precision.

Doubts related to the convenience of using constitutive parameters experimentally determined in the cutting process simulations have encouraged the development of different algorithms like Levenberg-Marquardt and Kalman filter dedicated to the constitutive parameters identification [21, 22]. These algorithms consist essentially on minimizing the mismatch between numerical and experimental results essentially due to the wrong definition of the material behavior. They are based on the use of the initial constitutive coefficients experimentally determined for the same tested material or even for another one from the same family [21, 22] in the definition of more accurate and suitable parameters well describing the material behavior and giving appropriate predictions. These involved inverse identification methods appear more interesting and reliable than the former one due to the fact that they allow reaching a better correlation with less cost. However, it is of major importance to note that inverse methods generally cause the time increase with the number of the identified parameters added to problems related to solution diversity resulting thus on a great distinction in terms of chip morphology, temperature distribution, and shear angle [1].

In fact, availability of many identification techniques presents the principle origin of this distinction in JC plastic parameters corresponding to the same material. To cut with this problem, many investigations have been done in the purpose to highlight the major role of appropriate material coefficients choice in numerical model reliability increase [9, 23, 24]. On the other hand, it is important to note that the JC model appears unable to reproduce alone chip formation and segmentation [25, 26] due to the fact that its expression exhibits a continuous increase of the flow stress-strain curve for whatever the strain and the temperature levels which does not represent the real workpiece material behavior. Hence, additionally to plastic model implementation, failure needs to be also defined especially when using the Lagrangian-based analysis. In examining literature review, we note that distinct fracture models have been developed in the purpose to precisely describe the damage produced during the machining process. However, the effect of the right definition of failure coefficients on the FE model reliability is still until now ignored and weakly understood by the majority of cutting modeling investigations.

In this study, the JC damage model coupled with the energy-based ductile criterion is defined to reproduce the Ti6Al4V behavior when failure is initiated in the material until its total fracture. These criteria already implemented in Abaqus/Explicit FE code have been widely used in conjunction with the JC plastic model. The main objective of this investigation is to increase as possible and with a minimum effort from the FE model reliability while studying the machining process of the Ti6Al4V alloy. The principal challenge of the present work is to improve from numerical simulation quality by only determining the most affecting JC parameters instead of modifying or defining new constitutive models with more coefficients number. To emphasize and point out the major impact of accurate rheological and damage parameters definition on the FE model reliability rise, a 2D orthogonal cutting model based on Lagrangian formulation is used. Careful comparisons between FE numerical predictions and experimental results taken directly from previous work [27] are made. Dependency of chip morphology, average cutting forces and temperature distribution to each rheological (A, B, n, C and m) and damage ($D_{1-5}$ and $G_f$) material parameters as well as to cutting speed definition is studied. From a scientific point of view, quantitative description of the predicted chip is required to improve the cutting process modeling while

highlighting its dependency to material constitutive laws definition. That is why segmentation frequency ($f_{seg}$), chip curvature radius ($R_c$), shear band spacing ($Ls$), chip serration sensitivity ($S_{seg}\%$), accumulated plastic strains within one segment of the numerical chip ($\Delta\varepsilon_{p(in\text{-}out)}$), and its serration intensity (CSI) are defined and carefully examined to enable and further a thorough parametric study of all the constitutive parameters. Numerical cutting forces are also compared with the experimental ones in order to get a benchmark model. This paper concludes that the adjustment of JC strain hardening coefficients ($A$, $B$, and $n$), thermal softening parameter ($m$), exponent fracture factor ($D_2$), and damage evolution energy ($G_f$) leads to interesting reduction in numerical model disagreement, while all the other constitutive parameters demonstrate almost a minor effect. This precision in determining the main causes of FE accuracy decrease is of vital interest since required time in parameters identification is deeply minimized thanks to the reduction in requested experimental tests and numerical iteration numbers.

## 2 Orthogonal cutting model

### 2.1 Numerical model definition

In order to analyze the effect of constitutive parameters definition on the cutting process, eventually on material separation and chip formation, a 2D orthogonal cutting model of the Ti6Al4V with assumption of plane strain conditions is developed with the FE software Abaqus/Explicit®. Explicit integration with fully coupled temperature-displacement conditions is assumed in all simulations because of its adequacy to high nonlinear problems like those faced in metal machining operation. Interaction between the cutting tool and the workpiece, model geometry changes added to material properties dependency to the loading conditions present the main origin of this encountered nonlinearity. Four-node elements mesh with linear interpolation, reduced integration, and automatic hourglass mode control (CPE4RT) are used in the discretization of both the cutting tool and the workpiece. These coupled elements take into consideration the effects of temperature and displacement variation during machining modeling. Relax stiffness hourglass control features is defined based on the results of Barge et al. [28] in order to control the nonphysical deformation modes generally related to Gauss point definition. Similar to the experimental test conditions, no cooling liquid is applied during Ti6Al4V machining modeling.

Lagrangian formulation is adopted where a multipart model is defined and the workpiece is divided into three tied parts as shown in Fig. 1 in the aim to allow chip generation with a maximum control of the elements mesh distortion problems. Definition of an intermediate thin layer permits a well control

of the material separation through the deletion of its totally damaged elements. Cutting tool motion results on the material separation where the upper part of the workpiece is transformed into chip while the bottom one corresponds to the finished material. In this study, an elasto-thermo-visco-plastic-damage behavior is defined to parts 1 and 2 of Fig. 1 while no damage is applied to part 3 located below the machined surface. Numerical cutting tool in tungsten carbide is considered as a rigid body where its thermal properties are implemented.

Achieving a sufficient accuracy of the cutting process modeling with reasonable time cost is generally required, that is why a mesh refinement is locally applied in order to properly reproduce shear bands formation, saw-toothed chip characteristics, and tool geometry specifications while reducing as possible from the computational time. Mesh element lengths about 5 and 10 μm are respectively defined around the cutting tool tip and in the intermediate-superior workpiece parts. These values are chosen after many mesh convergence tests which have been preliminary done in the purpose to guarantee both: (a) an interesting similarity between numerical and experimental chip morphology and (b) a reasonable computing time.

The basic model dimensions, geometry, and boundary conditions defined in this study are illustrated in Fig. 1. Cutting tool edge radius, rake, and flank angles are respectively equal to 20 μm, 2°, and 7°. The workpiece is supposed to be fixed in its bottom and both sides while the cutting speed is applied to the rigid tool which is constrained to move only in the vertical direction. Tested cutting speed, feed rate, and uncut chip thickness are the same applied by Calamaz in her experimental tests [27]. In addition to mechanical cutting conditions, a room temperature of 293°K is initially applied to the cutting tool and the workpiece. Along the machining process, it is yet Eqs. 8 and 10 which control the created and exchanged heat evolution in the workpiece and in the materials contact interfaces. Heat radiation and convection to the vicinity is ignored in this investigation due to the fact that they present a weak effect on numerical predictions since a very short cutting time simulation (about at maximum one millisecond) is defined which is not sufficient to obtain interesting heat exchange between the workpiece and the environment.

Note that the same material properties of the uncoated carbide tungsten cutting tool and the Ti6Al4V alloy workpiece than those defined by Calamaz in her investigation [27] are used where dependency to temperature variation is ignored.

### 2.2 Workpiece material modeling

The elasto-thermo-visco-plastic behavior of the machined material is described with the JC plastic law [29] which flow stress expression is given by Eq. 1. This model has been frequently used in metal machining modeling because of its

**Fig. 1** Numerical 2D orthogonal model geometry, boundary conditions, and heat exchange definition

adequacy to high non-linear problems like those accompanying the chip formation in addition to its reduced number of coefficients.

$$\sigma = \left[ A + B\overline{\varepsilon}_p^n \right] \times \left[ 1 + C\ln\left(\frac{\overline{\dot{\varepsilon}}_p}{\dot{\varepsilon}_0}\right) \right] \times \left[ 1 - \left(\frac{T - T_{ref}}{T_{melt} - T_{ref}}\right)^m \right]$$

(1)

where $\overline{\varepsilon}_p$, $\overline{\dot{\varepsilon}}_0$, $\overline{\dot{\varepsilon}}_p$, $T_{ref}$ and $T_{melt}$ are respectively the equivalent plastic strain, the reference plastic strain rate, the actualized plastic strain rate, the reference temperature, and the melt one of the workpiece. $A$, $B$, $n$, $C$, and $m$ are the JC plastic model parameters which corresponding values to the Ti6Al4V alloy are given by Table 1.

In order to model the material machining process with accurate prediction of the chip morphology, different strategies can be used. Either damage model definition [13, 15, 30–32] or strain softening consideration [9, 33–36] has been adopted in many investigations to reproduce material separation and shear bands localization within the chip thickness. In this paper and further to the JC plastic model definition, two distinct failure criteria are implemented is adopted where damage in the machined material is assumed to undergo two steps: (a) a failure initiation step (b) followed by its propagation up to the total fracture occurrence. For the first mode, the JC damage model [37] is used while for the second one, energy ductile failure criterion [38] is defined. The corresponding expressions of these two models are given by Eqs. 2–5.

$$D = \sum \frac{\Delta\overline{\varepsilon}}{\overline{\varepsilon}_f}$$

(2)

where $\Delta\overline{\varepsilon}$ presents the increment of updated plastic strain and $\overline{\varepsilon}_p$ is the equivalent plastic strain in the damaged element

expressed by Eq. 3. It is given as a function of stress triaxiality $\sigma^*$ (equals to the ratio of hydrostatic to Von Mises stresses $\sigma_h/\sigma_{VM}$), strain rates $\overline{\dot{\varepsilon}}_p$, and temperatures $T$. Note that failure is initiated in the material when the actualized state variable $D$ is equal to the unity.

$$\overline{\varepsilon}_f = \left[ D_1 + D_2 \exp\left(D_3 \sigma^*\right) \right] \times \left[ 1 + D_4 \ln\left(\frac{\overline{\dot{\varepsilon}}_p}{\dot{\varepsilon}_0}\right) \right]$$
$$\times \left[ 1 + D_5 \left(\frac{T - T_{ref}}{T_{melt} - T_{ref}}\right) \right]$$

(3)

where $D_i$ ($i = 1, 2, 3, 4, 5$) are the JC material fracture parameters and its corresponding values to Ti6Al4V alloy are presented in Table 2.

In this paper, damage evolution $D_{ev}$ is introduced in the aim to reproduce the progressive degradation of material stiffness. The implementation of this criterion allows avoiding mesh dependency problems [40] due to the fact that it describes material failure behavior no more as a stress-strain response but as a stress-displacement one. It is recommended to adequately define the damage evolution modes since for the case of 2D and plane strain orthogonal cutting conditions (which is the case of this investigation), only two fracture modes exist according to [30, 41]: (1) the opening mode and (2) the sliding one which correspond respectively to the tensile and the shear

**Table 2** JC damage coefficients values corresponding to the Ti6Al4V [20, 39]

| JC damage coefficients | | Value |
|---|---|---|
| Initial failure strain | $D_1$ | −0.09 |
| Exponent factor | $D_2$ | 0.25 |
| Triaxiality factor | $D_3$ | −0.5 |
| Strain rate factor | $D_4$ | 0.014 |
| Temperature factor | $D_5$ | 3.87 |

modes. This well explains, according to Miguelez et al [42], the noted differentiation in material triaxiality, and consequently in failure levels, between the chip (part 1) and the passage tool zone (part 2). For this reason, exponential damage evolution (Eq. 5) with higher failure energy value is applied to the upper part of the workpiece transformed into chip. However, a linear damage evolution (Eq. 4) with less pronounced energy value is defined to part 2 since it is not the same mechanical phenomena involved when modeling the material separation and its partial slide away above the formed ASBs.

$$D_{ev.L} = \frac{\overline{u}_p}{\overline{u}_f} = \frac{L\overline{\varepsilon}_p}{\overline{u}_f} \tag{4}$$

$$D_{ev.exp} = 1 - \exp\left(-\int_0^{u_{pf}} \frac{\overline{\sigma}}{G_f} d\overline{u}_p\right) \tag{5}$$

where $\bar{u}_p$ and $\overline{\varepsilon}_p$ are respectively the equivalent plastic displacement and strain. $L$ presents the characteristic length of the quadrangular element mesh edge and its introduction in plastic displacement definition causes a mesh element size dependency reduction. $\bar{u}_f = 2G_f/\sigma_y$ is the equivalent plastic displacement in totally fractured material where $G_f$ presents the fracture energy given by Eq. 6. Its expression in the case of 2D strain plane conditions is given as a function of the fracture toughness ($K_c$), the Poisson's ratio ($\gamma$), and the Young's modulus ($E$) of the machined material according to Mabrouki et al. [30]. $\sigma_y$ is the yield stress of the machined material.

$$(G_f)_{I,II} = \frac{(1-\nu^2)}{E}\left(k_c{}^2\right)_{I,II} \tag{6}$$

The subscripts $I$ and $II$ correspond respectively to the opening and the shearing modes. Whatever the damage evolution mode, flow stress tensor in failed element $\sigma$ is described by the following Eq. where $\tilde{\sigma}$ corresponds to the stress state when no damage occurs in the solicited material [43].

$$\sigma = (1-D_{ev})\tilde{\sigma} \tag{7}$$

As material removal mechanism is generally accompanied by a heat generation because of the interesting levels of involved friction (Eq. 10) and mechanical plastic deformation of the solicited material (Eq. 8), this generated heat is accompanied by an important temperature raise within the workpiece and the cutting tool. Fraction of energy produced in the case of difficult-to-cut material by its plastic work $\eta_p$ is usually ranged from 0.85 to 0.95 according to Shet and Deng [44] and is assumed to be equal to 0.9 in the current work.

$$\dot{q}_p = \eta_p \overline{\sigma} : \dot{\varepsilon}_p \tag{8}$$

## 2.3 Workpiece-cutting tool interaction definition

In addition to numerical model definition and material behavior description, both mechanical and thermal contact properties need to be carefully implemented due to the fact that they heavily influence on the FEM results according to Özel [45]. In fact, an accurate definition of the friction taking place between the cutting tool and the machined material is crucial in machining modeling due to the fact that it controls the heat distribution, the temperature levels, the material flow, and the cutting tool wear mechanisms. Despite the availability of many friction models in literature review [45, 46] varying from few to very complicated, the accurate prediction of material contact is still until now a main challenge accompanying that metal cutting process. Friction involved between the cutting tool and the workpiece are not yet totally understood since it is greatly dependent on multiple variables (like temperature and chip sliding speed). According to previous investigations [9, 46], except temperature distribution, all the other numerical outputs are weakly affected by friction definition. Consequently, for more simplicity and basing on recent studies [9, 25, 41], Coulomb and Tresca models are coupled and used in this paper. This simultaneous dependency to both normal and shear friction stresses (as expressed by Eq. 9) permits the reproduction, with more simplicity, of the sticking and sliding contact conditions taking place between the cutting tool and the machined material. Around the cutting tool tip, a strong material adhesion occurs resulting on very interesting pressure levels while faraway the tool tip, machined material easily slides in front of the tool faces. This distinction in contact types is followed by various pressure levels, from the cutting tool edge to the point where no more contact takes place, as justified in [47].

$$\begin{aligned} &\text{If } \mu \times \sigma_n < \tau_{max} \text{ Then } \tau_f = \mu \times \sigma_n \\ &\text{If } \mu \times \sigma_n \geq \tau_{max} \text{ Then } \tau_f = \tau_{max} = m_{Tresca} \times k \end{aligned} \tag{9}$$

where $\mu$, $\sigma_n$, $m_{Tresca}$, and $k$ are respectively the Coulomb's friction coefficient, the normal stress, the Tresca factor, and the shear flow stress.

During Ti6Al4V alloy machining, interaction between the cutting tool and the workpiece leads to the generation of an interesting heat. Heat flow created by materials friction ($\dot{q}_f$) is described by the following relation (Eq. 10). All this energy is assumed to be converted into heat and equally absorbed by the materials in contact. Heat conduction flux is neglected in this investigation because the lack of experimental value corresponding to the tested materials couple and cutting conditions in [27].

$$\dot{q}_f = \eta_f \times \tau_f \times V_s \text{ and } \dot{q}_{\to Tool} = f_f \dot{q}_f \tag{10}$$

where $\eta_f$, $\tau_f$, $V_s$, and $f_f$ are respectively fraction of the energy generated by friction work and converted into heat, friction

stress, material sliding velocity, and fraction of the heat transmitted to the cutting tool. $\dot{q}_{\to Tool}$ is the heat flux created by material friction and gone to the cutting tool.

# 3 Numerical results and discussions

## 3.1 Chip morphology and cutting forces dependency to the JC plastic parameters definition

As already demonstrated in previous investigation [27], machining process of the biphasic Ti6Al4V titanium alloy is generally resulting on a segmented chip formation, even at relatively low cutting speeds. Meanwhile, it is of high importance that the numerical model accurately reproduces this specific chip morphology due to the fact that it greatly affects the whole cutting process. However, to achieve a best agreement between numerical and experimental results, an adequate definition of thermo-elasto-visco-plastic behavior of the machined material is required. Due to the availability of many JC plastic parameters corresponding all to the same tested material (as reported in Table 1), a preliminary study focusing on determining the most suitable parameters set well reproducing the machined material behavior is done. In this section, only JC parameters sets with a value of $A$ approximately (±25 %) equal to the initial yield stress of the studied Ti6Al4V alloy determined in ambient temperature ($A = \pm 25\% \sigma_y$) are compared. The most suitable set able to give a best agreement with the experimental listed [27] is kept in the next parts.

It is worth noting that for the same strain rate, flow stress curve described as a function of the strain and the temperature exhibits a clear distinction in its evolution where reached levels strongly differ from one JC plastic parameters set to another (see Fig. 2). In fact, the effect of this diversity on machining process in terms of material separation mechanism, chip morphology, and cutting forces obtained under the same cutting conditions needs to be clarified.

A first correlation between numerical chip serration characteristics and cutting forces levels has been established in the current section. The effect of JC coefficients definition on these two parameters has been examined due to the fact that they greatly carried the aptitude of the FE model in well reproducing the cutting process phenomena. When comparing predicted chip morphology resulted from the definition of different JC plastic sets and obtained under moderate even high cutting speeds, a serrated chip with obvious difference in its curvature radius ($R_c$), shear bands spacing ($L_s$), and segmentation frequency ($f_{seg} = V_c/L_s$) has been simulated. The choice to quantify chip serration through the check of its characteristics is justified by the fact that they give a clear idea about its morphology. Figures 3 and 4 highlight that a more curved chip is formed when JC hardening modulus B has been

reduced with whatever the cutting speed value. This result emphasis that $R_c$ depends not only on the cutting tool rake angle as concluded by Atlati et al. [48], or on mesh density and FE formulation definition like stated in [49], but also on material behavior description. A combination of Figs. 2 and 3 confirms that flow stress definition affects the chip morphology which becomes more saw-toothed as reached levels of the flow stresses are higher. On the other hand, a low chip serration has been obtained with JC-d and JC-e sets which is due to the reduction in the hardening modulus value as demonstrated in the next section. However, with a cutting speed equal to 180 m/min, numerical chip has exhibited less distinction in its formed saw-teeth for different JC sets as shown in Fig. 4. Almost no change has been noted in the chip segmentation frequency as well as in the shear band spacing for this $V_c$. This result can be attributed to the dominant effect of cutting conditions on chip serration in regard to plastic parameters definition.

Figure 5 shows a well correlation between the onset of the ASB and its total formation, in one hand, and the cutting forces minimum and maximum, on the other hand. It has been highlighted that the onset of a new ASB is accompanied by a pronounced load applied to the cutting tool. However, this latter is subjected to less pronounced forces when the machined material partially slides away from the upper surface of the workpiece within the totally formed shear band and leads consequently to a few materials in contact with the cutting tool. This means that every cutting forces drop corresponds to a completely formed ASB and vice versa. Another result related to plastic model definition has been noted where for the same cutting conditions, average shear bands spacing corresponding to the distance between two consecutive ASBs, is weakly varied from one JC set to another, except with JC-d set. With the application of this latter, one more saw-tooth has been formed for the same machined material length and has contributed to a drop in the average $L_s$ value, so to an increase in the chip serration frequency (see Fig. 6). Even with the same simulation, a slight modification in $L_s$ value has been pointed out. It is presented by the delay (or an acceleration) in tangential forces drop and consequently in a new ASB formation as stated by Fig. 5.

Furthermore, it is possible to link between average cutting forces disagreement and chip morphology mismatch. For a cutting speed equal to 75 m/min, a well saw-toothed chip compared to the experimental one is accompanied by a negligible mismatch in tangential forces prediction (see Figs. 3(b, c, and f) and 7). In fact, the right definition of JC constitutive coefficients leads not only to a high accuracy in numerical chip morphology but also to a well correlation in term of tangential forces $F_c$ prediction. Moreover, it is demonstrated that simulated cutting forces follow the same trend of the shear bands spacing where a decrease in $L_s$ is accompanied by a reduction in the average simulated $F_c$ (as highlighted in
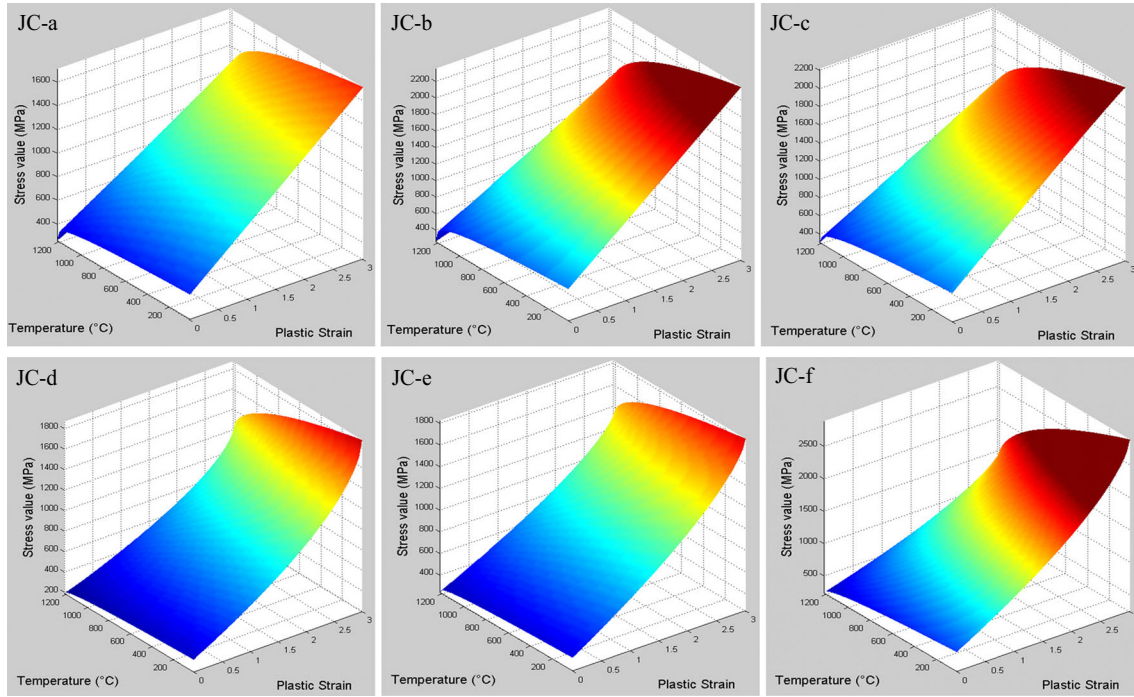
**Fig. 2** Flow stress evolution with the temperature and the strain rate corresponding to different plastic JC sets ($\dot{\varepsilon} = 10^4 \text{ s}^{-1}$)

Figs. 6 and 7a). However, an underestimation in feed forces $F_f$ has been obtained especially when the cutting speed is raised from 75 to 180 m/min. In this regard, we can cite that an increase in $V_c$ has contributed to a negligible rise just of 20 N in simulated $F_f$ contrarily to the experimental results [27] where a difference nearly about 120 N has been noted. Moreover, with whatever moderate or high cutting speed, $F_f$ is generally in bad agreement with the experimental one especially at high cutting speeds. This disagreement is related to the deletion of damaged elements mesh located just around the cutting tool edge and subjected to extremely high loading conditions. This method is associated to Lagrangian formulation assumption initially made which requires the use of a specific failure model and the predefinition of an adequate critical damage value. However, with real cutting tests, crack takes place in the machined material and results on micro-
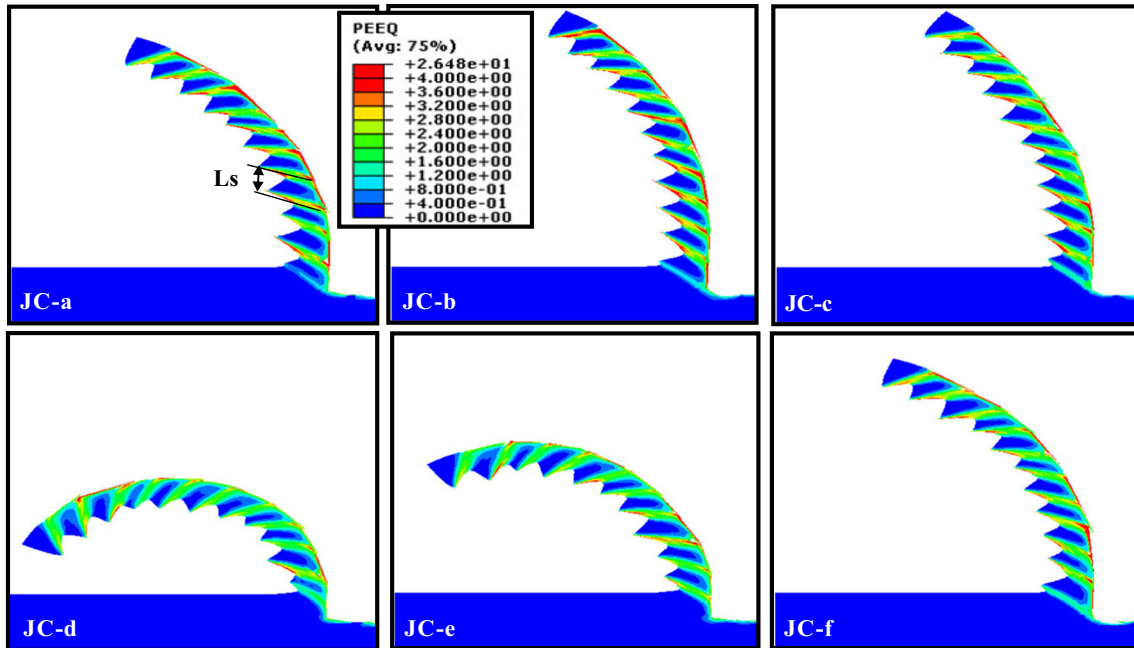


**Fig. 3** Chip morphology and strain evolution dependency to JC plastic parameters ($V_c = 75$ m/min, $a_p = 3$ mm, and $f = 0.1$ mm/rev)
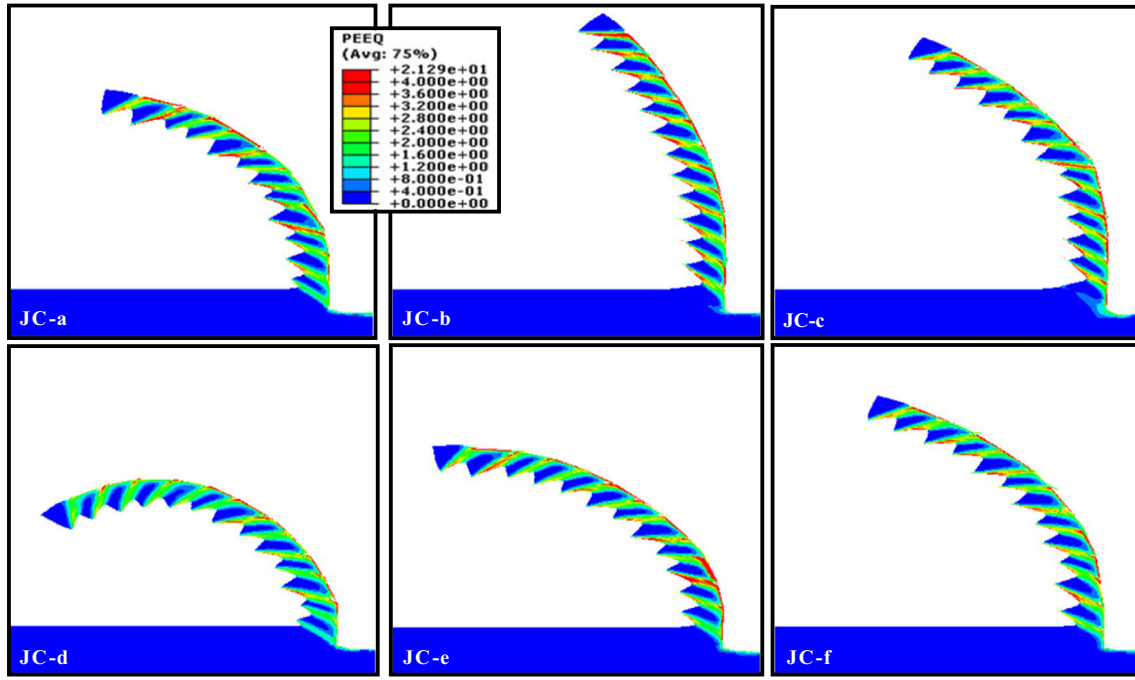
**Fig. 4** Dependency of the chip morphology and the equivalent plastic strain evolution to JC plastic coefficients ($V_c = 180$ m/min, $a_p = 3$ mm, and $f = 0.1$ mm/rev)

fractures propagation within a very small Ti6Al4V microstructure known by its limited grains size (about few micrometers as listed in [50]). An additional possible explanation about this mismatch in $F_f$ prediction is the adopted JC plastic model which cannot accurately reproduce the material work hardening sensitivity to either moderate or high strain rates.

Despite of this mismatch in $F_f$ prediction, it is important to underline that the accurate definition of the JC plastic model

parameters has contributed to a reduction in the disagreement between numerical and experimental feed forces even if it is negligible and it is not in the same order of $F_c$ and chip morphology amelioration. For example, with the definition of a moderate cutting speed, calculated error in terms of tangential and feed forces was passed respectively from about 13 and 31 % when the JC-d set is used to just about 2 and 16 % respectively when JC-f coefficients are defined. Definition
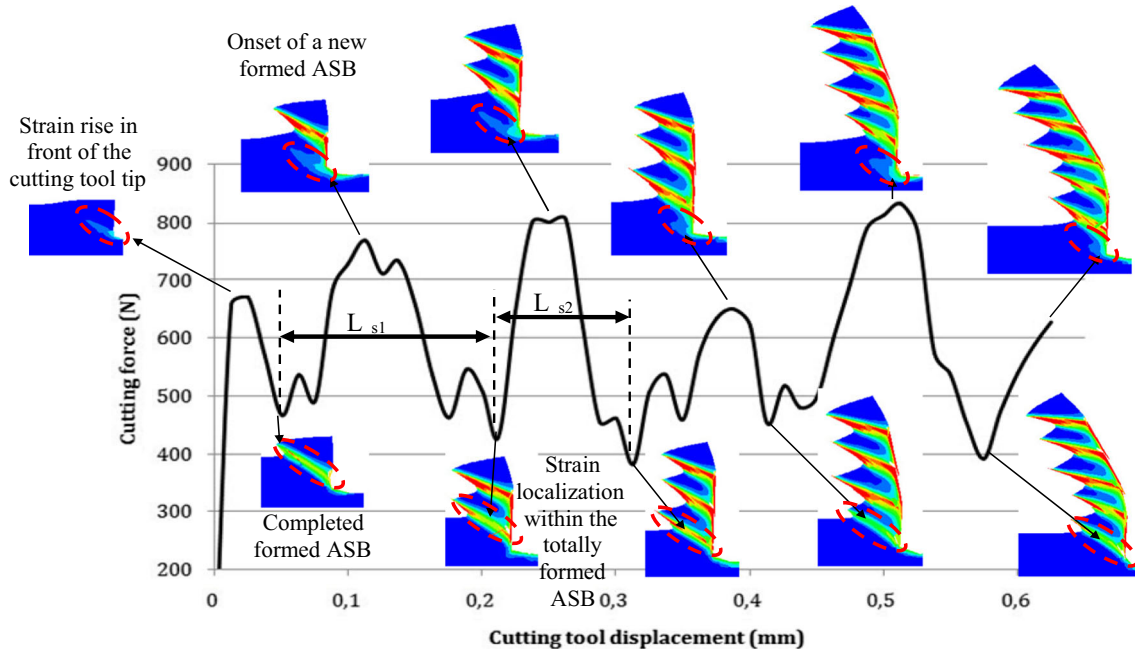


**Fig. 5** Link between numerical cutting forces evolution and ASB formation (case of JC-f parameters set definition)
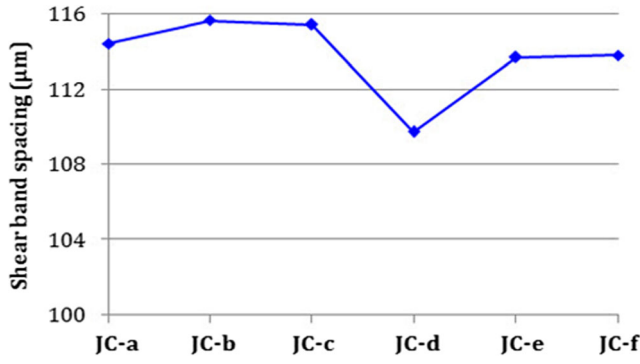
Fig. 6 Shear band spacing ($L_s$) evolution for the six tested JC coefficient sets

of this JC set has contributed to the formation of well segmented chip similar to the experimental one. In fact, even if JC rheological parameters cannot offer enough accuracy in terms of feed forces, the application of JC-f set remains much improving from the global FE model accuracy instead of the other tested JC set. In fact, JC coefficients given by the last line of Table 1 are kept and used as the original plastic parameters in next sections.

## 3.2 Parametric study of the JC plastic model effect on shear bands localization and cutting forces sensitivity

As it has been recently reported, FE simulations of the cutting process presents an effective tool of local information access, cost reduction, and understanding amelioration of the chip formation once it is accurately defined. It has been highlighted in a previous section that metal cutting modeling performance depends on the method used to deal with JC parameters identification. However, the ambiguity related to material plastic coefficients effects (as well as the damage one) is still not yet solved unless the principle responsible and origin of obtained mismatch between experimental and numerical results is not precisely determined. Face to this problem, determination of the relationship between machining simulation outputs

and every constitutive parameter presents a vital pre-request. A parametric study of the JC model, where the effect of its coefficients on cutting modeling has been separately studied, could be considered as of extremely high interest. This investigation focusing on highlighting the most dominant JC parameters has as main goal to help not only in specifying FEM miscorrelation causes, but also to improve as possible from numerical model accuracy when specific causes of numerical results miscorrelation are previously known.

In this section, JC plastic coefficients are separately varied in a range of ±25 % from their original values given by Table 1 (JC-f). Contrarily to the previous section, no more mixed changes are done in order to determine the role of every JC coefficient and to highlight the most affecting ones mostly controlling the machining modeling reliability. The focused aim is to emphasize problems related to the wrong definition of the most dominant plastic coefficients in regard to others. In this study, in addition to numerical chip curvature radius ($R_c$), shear band spacing ($Ls$), and segmentation frequency ($f_{seg}$) definition, dependency of the chip serration sensitivity factor ($S_{seg}\%$), the accumulated plastic strain in one formed sawtooth ($\Delta\varepsilon_{p(in-out)}$), and the chip serration intensity (CSI) to JC coefficients ($A$, $B$, $n$, $C$, and $m$) has been carefully investigated. Effect of every plastic parameter in cutting and feed forces prediction has been also examined.

The first remark to signal is that, in agreement with previous conclusion, hardening modulus ($B$) is one of the main JC plastic parameter controlling the chip curvature where a reduction in its radius value $R_c$ is obtained with the definition of low $B$ value. It is also deduced from Fig. 8 that any increase in either initial yield stress ($A$) or thermal softening coefficient ($m$) has resulted on a great change in the same way of chip curvature radius. In fact, susceptibility of the machined material to curl on itself is affected by the accurate definition of JC strain hardening and thermal softening terms. Referring to Fig. 8, a pronounced change in chip shape, geometry, and curvature radius is associated to the variation in initial yield stress value while a negligible effect related to strain rate
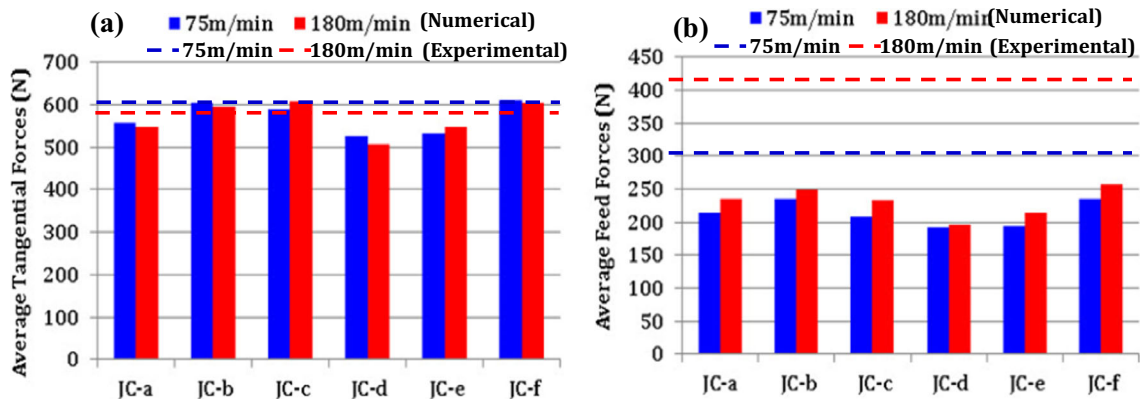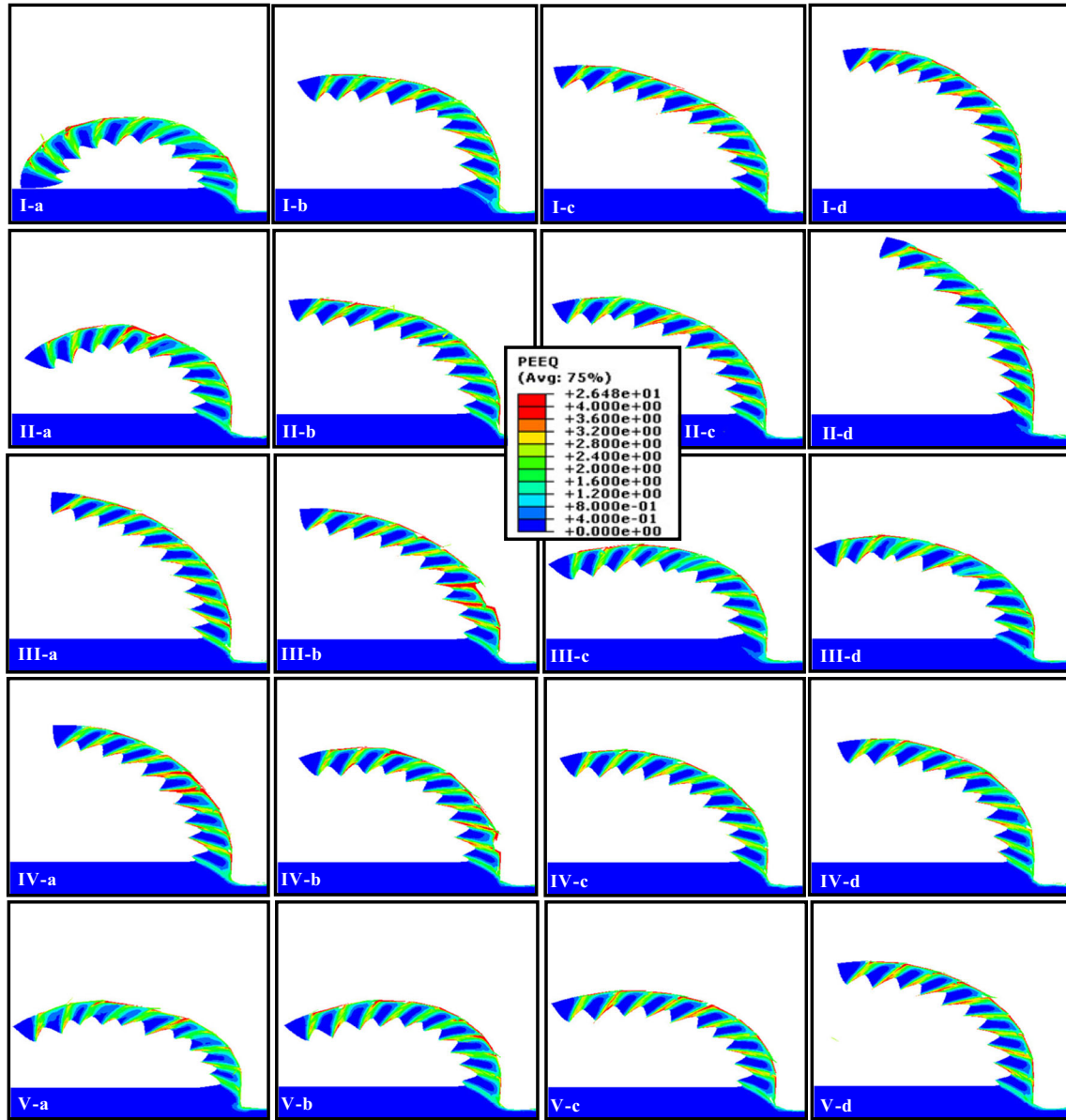


Fig. 7 Dependency of the average cutting (a) and feed (b) forces to JC plastic parameters with respect to the cutting speed

**Fig. 8** Chip serration dependency to every JC plastic parameter for a cutting speed of 75 m/min (*I*, *II*, *III*, *IV*, and *V* refer to JC plastic coefficients (*A*, *B*, *n*, *C*, and *m*, respectively) while *a*, *b*, *c*, and *d* correspond to the range of their variations (−25, −10, +10, and +25 %, respectively))

dependency coefficient (*C*) change (for the case of the tested material) has been signaled. Nevertheless, strain hardening exponent (*n*) has demonstrated an inverse trend where the more its value is decreased, the more the chip is curved and thicker but less segmented.

Figure 8I (a–d) presents the effect of the initial yield stress value variation while maintaining constant all the other JC plastic coefficients. In general, the tendency of the chip to be well serrated was increased as *A* becomes more important. This pronounced segmentation is essentially due to the fact that simulated material is generally hardest to machine under important initial yield stresses. Additionally, its plastic deformation starts late and at relatively elevated flow stresses levels before it goes along the removed material thickness. This

phenomenon encourages material slide away from the free surface of the workpiece. In fact, a well formed ASB is simulated as a consequence of the high plastic strain noted within. The same tendency is pointed out when raising the hardening modulus value but with less pronounced changes. The increase in *B* has experienced a rise in the magnitude of the plastic strain located in the primary shear zone. This result can be explained as reported in Fig. 9 to the reduced effect of *B* on flow stresses levels compared to *A*.

It is underlined that an investigation based only on studying the evolution of chip curvature radius, shear band spacing, and segmentation frequency cannot be considered as sufficient due to the fact that these parameters just give in general a global information about chip morphology without any

**Fig. 9** Flow stresses evolution for different initial yield stress (*A*) and hardening modulus (*B*) ($T° = 773°$K and $\dot{\varepsilon} = 4.10^4$ s$^{-1}$)
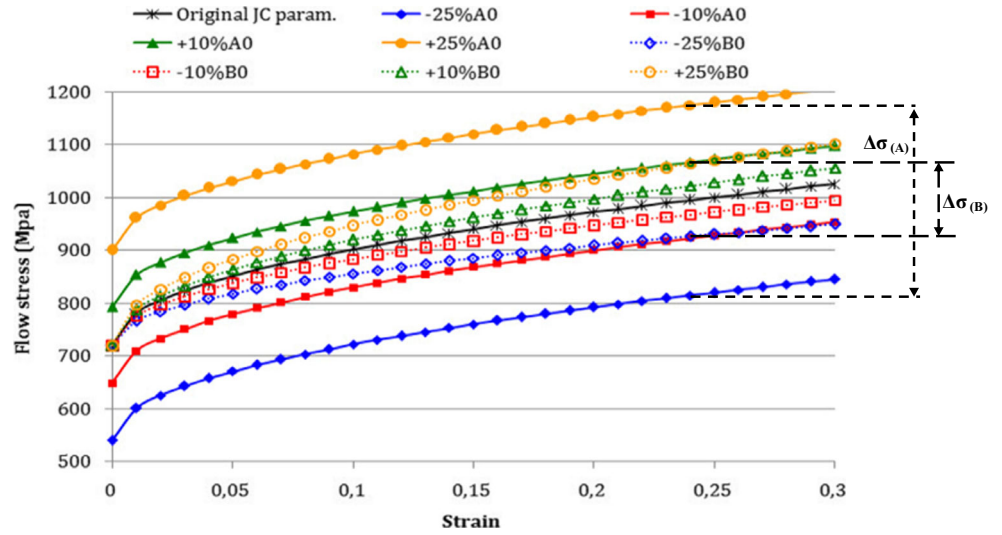
precision in the description of its segmentation localization and strain evolution. Additionally, from a point of view that chip formation mechanism and its morphology characteristics play a major role in numerical model predictions (like cutting forces, temperature levels, finished surface quality, tool wear, failure modes), more precious characterization of the removed material geometry is required. For this reason, chip serration sensitivity factor ($S_{seg}\%$) is defined (see Eq. 11). It is given as a function of the initial and the modified chip segmentation degree ($G_{seg0}\%$ and $G_{seg1}\%$, respectively), and it describes the intensity of the produced serration where the more the formed saw-tooth is pronounced, the less the ratio of valley (*h*) to peak (*H*) chip thickness, so of the $G_{seg}\%$, is relevant. Consequently, the difference between $G_{seg1}\%$ and $G_{seg0}\%$ is decreased and results on the reduction of $S_{seg}\%$. Meanwhile, obtaining a very low or high value of $S_{seg}\%$ means that the changed JC coefficient has a dominant effect on the chip segmentation control. Figure 10 illustrates that the variation in initial yield stress and hardening modulus values have demonstrated a heavy decrease in the chip segmentation sensitivity factor when *A* or

*B* has been increased. This result is explained by the less susceptible of the machined material to undergo a plastic deformation resulting on a well chip serration. The inverse trend obtained with the strain hardening exponent increase is however attributed to the fact that when interesting *n* value, the thermoplastic material instability phenomenon is accelerated and contributes to an easy deformation of the machined material. Consequently, less difference between the peak and the valley chip thicknesses was obtained. The same explanation can justify this reduction in chip segmentation following the definition of low thermal softening coefficient.

In fact, this study has demonstrated that thermoplastic instability presents one of the most responsible parameters that control the ASBs formation. Moreover, the underestimation of *m* (*n*) has exhibited a fast (slow) dominance of the thermal softening in regard to the hardening effect giving rise to a drop (an increase) in material hardening capacity. While, the overestimation of *m* (*n*) has contributed to a delay (acceleration) in the thermoplastic instability occurrence accompanied by the requirement of more stresses to plastically deform the solicited
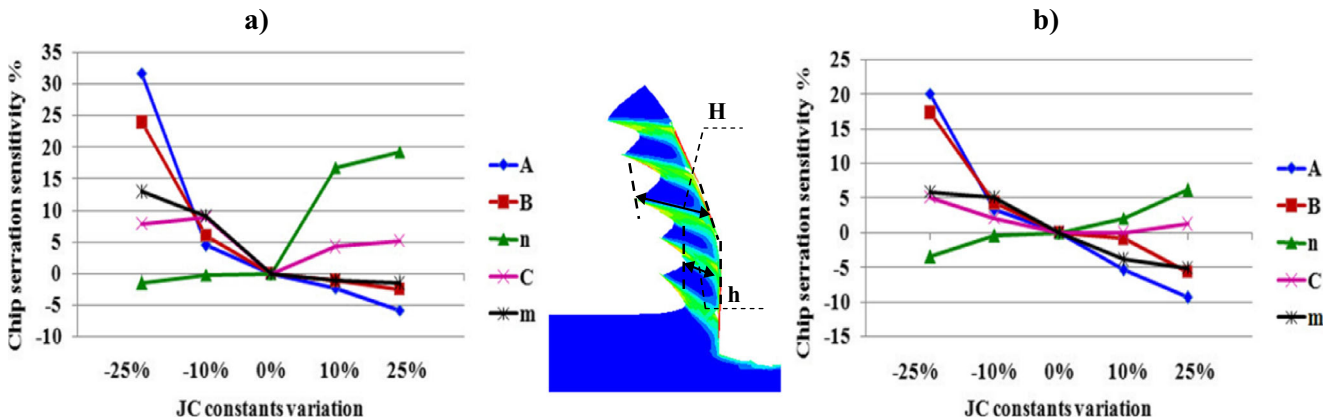


**Fig. 10** Chip segmentation sensitivity factor dependency to JC plastic coefficients definition under different cutting speeds (**a** $V_c = 75$ m/min and **b** $V_c = 180$ m/min)

material. Presented findings are in well correlation with the Chen and al [20] conclusions stating that thermal softening is generally dominant within the shear bands while outside these bands, it is rather the effect of strain hardening which becomes more pronounced. Meanwhile, varying one of thermal or strain hardening parameters should directly affect the chip segmentation intensity.

An examination of temperature levels and propagations along the chip thickness is done in order to explain the pronounced chip segmentation obtained with the rise of the initial yield stress and the hardening modulus. Figure 11 demonstrates that interesting temperature levels are propagated within the primary shear zone until achieving the free side of the chip when the implemented value of either $A$ or $B$ has been increased (Fig. 11). This temperature rise became more remarkable with an over increase in the initial yield stress value and it is accompanied by a well chip segmentation. Consequently, the more $A$ is important, the more the level of the strength acquired by the machined material is important, the more it is hard to plastically deform the workpiece. As a result, more consumed energy is required and is converted into heat which well explains this rise in simulated temperature.

$$S_{Seg}(\%) = 100 \times \left( \frac{G_{Seg1}\% - G_{Seg0}\%}{G_{Seg0}\%} \right) \text{ where } G_{Seg}{}^0/_0$$

$$= 100 \times \left( {}^h/_H \right) \qquad (11)$$

$G_{seg}\%$ is the chip segmentation degree obtained with specific JC constitutive coefficients combination. $H$ and $h$ are respectively the average peak and valley chip thickness schematized in Fig. 10.

Findings of the present work are compared with the fewest ones available in literature where the same tendencies have been highlighted by Wang and Liu [51]. Authors have demonstrated that the chip bending factor is decreased with the decrease of either $A$ or $B$ and increased when $n$ is increased. Moreover, it has been concluded in their study that JC strain rate dependency coefficient presents a negligible effect on the chip morphology prediction which is the same result found in this study. Nonetheless, the rise in thermal softening parameter has resulted according to the authors on more pronounced changes in chip segmentation in the sense of its reduction which is not the case with the current investigation.

A verification step is done where higher cutting speed (180 m/min) is tested while maintaining the same depth of cut and feed rate. In general, chip geometry dependency to the pre-specified JC plastic parameters has shown a great similarity under both moderate (75 m/min) and high cutting speeds (180 m/min). Figure 10 demonstrates that with the definition of 180 m/min, the increase in $A$, $B$, $n$, and $m$ values has led to the same pointed trend but with less pronounced distinction in the chip segmentation sensitivity factor. This result is essentially due to the dependency of the average peak and valley chip thicknesses to the defined cutting speed, similarly to the experimental chip (see Fig. 12). Meanwhile, the application of different cutting conditions does not demonstrate any contradiction with previous deduction concerning the role of every JC parameter. The same trends related to $S_{seg}\%$ dependency to constitutive coefficients are kept as summarized in Fig. 10.

In the aim to more understand the role of cutting speed on the machining process and especially on the chip segmentation phenomenon, evolution of numerical local plastic strain measured in and out the formed shear bands ($\varepsilon_{p(in)}$ and $\varepsilon_{p(out)}$ respectively) along the mid-thickness of the chip has been plotted. These measurements help in quantifying the local deformation within the removed material. Note that a maximum plastic strain ($\varepsilon_{p(max)}$) is measured in the formed ASBs while a minimum one ($\varepsilon_{p(min)}$) is located out the shear bands especially in the dead zone of the numerical chip.
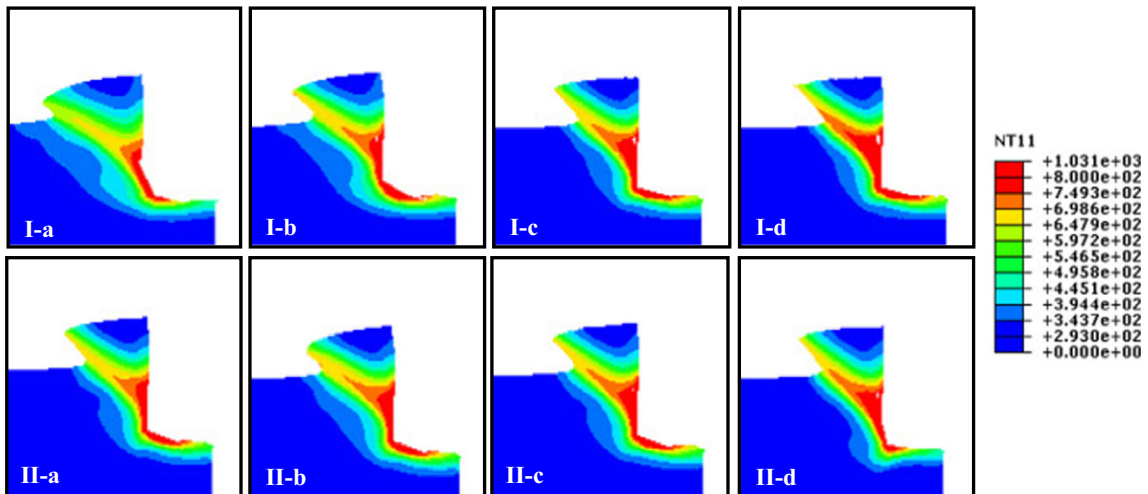


**Fig. 11** Temperature evaluation within the primary shear zone under different value of $A$ (I) and $B$ (II) ($a$ −25, $b$ −10, $c$ +10, and $d$ +25 %)

**Fig. 12** Comparison between numerical (*II*) and experimental (*I*) chip morphology obtained under different cutting speeds: **a** 75 m/min and **b** 180 m/min
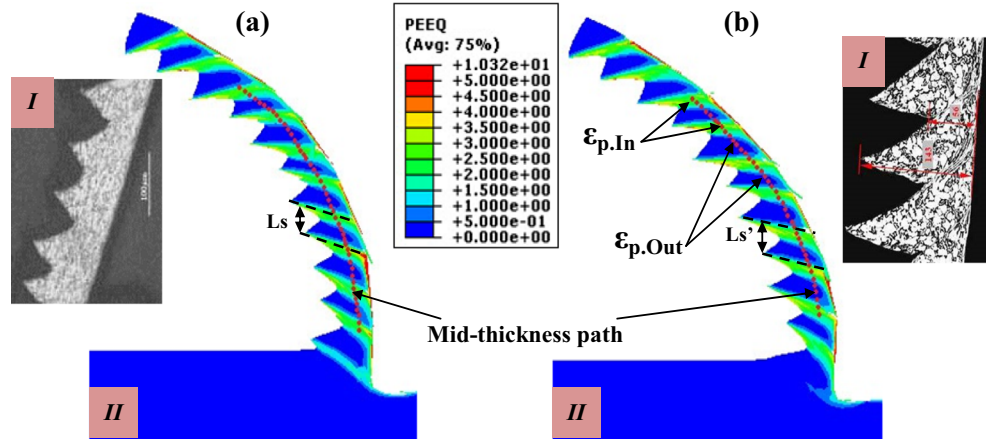
Figure 13 highlights an increase in the accumulated plastic strain $\Delta\varepsilon_{p(in-out)}$ when cutting speed has been raised (equals to 180 m/min). A chip serration intensity (CSI) is introduced in this investigation. It is defined as a ratio of $\Delta\varepsilon_{p(in-out)}$ to $\varepsilon_{p(out)}$ (CSI $= \Delta\varepsilon_{p(in-out)}/\varepsilon_{p(out)}$). The definition of this parameter permits to study the dependency of local strains to the cutting speed and to demonstrate its effect on the saw-toothed material. For almost a constant $\varepsilon_{p(out)}$, CSI has exhibited a reduction in its value as a low cutting speed has been defined. This sensitivity is attributed to the rise in the heat generated by material plastic deformation when high cutting speeds are defined leading to more compressed chip, for the same feed rate *f*, with low average valley chip thickness. Additionally, deducted strain evolution along the chip mid-thickness has demonstrated dependency of the shear spacing to the cutting speed where a delay in plastic strain drop (or increase) is obtained as $V_c$ is increased. Consequently, chip segmentation frequency is also affected. Comparison with previous studies of the literature review has been done and has demonstrated a well correlation in terms of chip serration frequency. Experimental tests of Sun et al. [50] focused on studying the behavior of Ti6Al4V alloy under different cutting conditions have pointed out that frequency of the saw-tooth formation is

essentially increased by the cutting speed rise or the feed rate reduction.

Cutting and feed forces dependency to JC plastic coefficients and cutting speeds has been additionally studied. Figures 14 and 15 illustrate the average $F_c$ and $F_f$ obtained under two cutting speeds (75 and 180 m/min) and with the application of distinct JC parameters. In correlation with previous findings concerning chip segmentation, the strain rate dependency coefficient has demonstrated its fewest effects on cutting forces variation. However, the increase in JC initial yield stress and JC hardening modulus value has been followed by an increase in the predicted average cutting forces. This result can be explained by the low curved chip simulated with high value of *A* or *B* which means that much material becomes in contact with the cutting tool and results on numerical forces increase. Concerning the rise in average $F_c$ value following the variation of *m* in the same sense, it is also due to the less pronounced curvature radius. By contrast, cutting forces drop accompanying the work hardening exponent rise is probably attributed, as for chip segmentation decrease, to the acceleration in thermoplastic instability phenomenon.

Nevertheless, the increase in the cutting speed has resulted on more pronounced change in numerical tangential forces

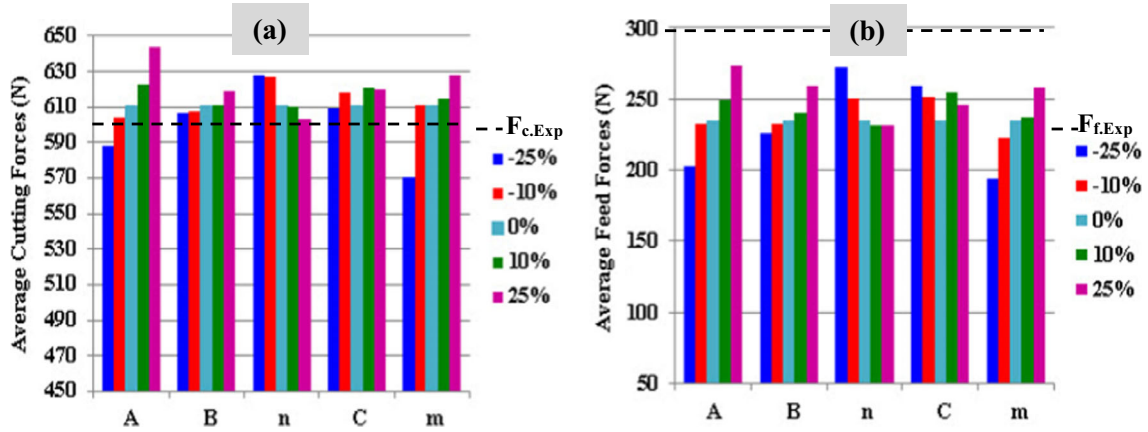**Fig. 13** Dependency of the equivalent plastic strain evolution to the cutting speed
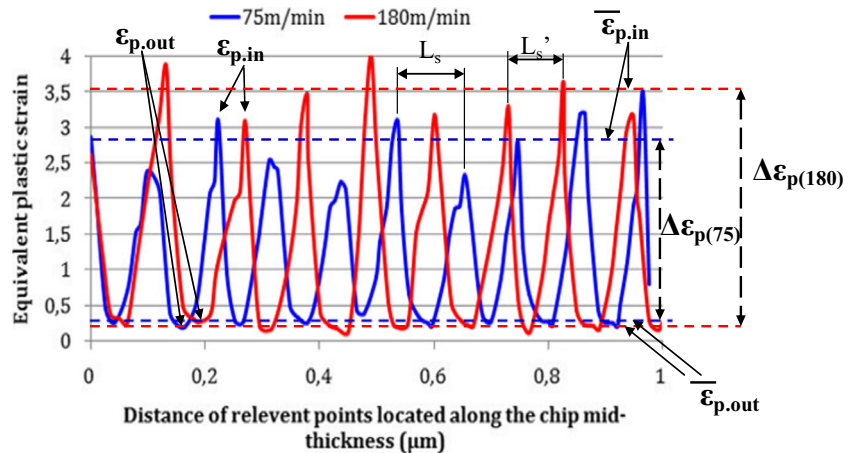
**Fig. 14** Parametric study of the JC plastic model effect on cutting and feed forces ($V_c = 75$ m/min, $a_p = 3$ mm, and $f = 0.1$ mm/rev)

when JC plastic constants have been varied as reported in Fig. 15. The initial yield stress and the thermal softening coefficient appear as the most influencing on numerical forces prediction compared to the rest of JC plastic parameters for whatever the cutting speed. A variation about ±25 % of the $A_0$ and $m_0$ values has led to a negligible increase in average $F_f$ which did not exceed 15 and 10 % respectively when an important speed has been applied to the cutting tool (180 m/min). Whereas, when a moderate cutting speed (75 m/min) is defined, predicted $F_f$ prediction has been varied within more important ranges. A calculated error of about 29 % and 27 % when the value of A and m has been respectively raised is obtained. Even if these two JC coefficients have demonstrated a great importance in feed efforts prediction when a moderate cutting speed is applied, this does not exclude that hardening modulus as well as work hardening exponent need also to be accurately determined to guarantee interesting reliability of the FE model. This seems logical because of the dependency of the machined material strength to its hardening and thermal softening properties controlled by the JC plastic coefficients: $A$, $B$, $n$ and $m$. This result is in correlation with the conclusions of Zhang et al. [39] who have also concluded that the use of higher hardening parameters leads to a direct impact in

machining modeling in terms of chip morphology and cutting forces.

**3.3 Effect of damage model parameters in FE prediction**

Because of damage initiation and propagation need to be accurately described in conjunction with material plastic definition, another investigation focalized in failure parameters effect is done in this section. In the same way to the previous study (Section 3.2), a separate variation in the value of every failure constant ($D_i$ as well as $G_f$) in a range of ±25 % from its initial value has been done in the aim to highlight the most influencing ones on machining modeling. Predicted cutting forces and chip morphology resulting from the increase or the decrease in damage coefficients value have been compared with original results obtained with the application of initial damage parameters. In this section, only the effect of damage coefficients is discussed hereafter while keeping as constant all the JC plastic parameters.

Figure 16 reproduces dependency of the chip morphology to only JC damage parameters while Fig. 17 illustrates the effect of failure energy evolution definition. When JC damage coefficients have been varied in the tested ranges, chip
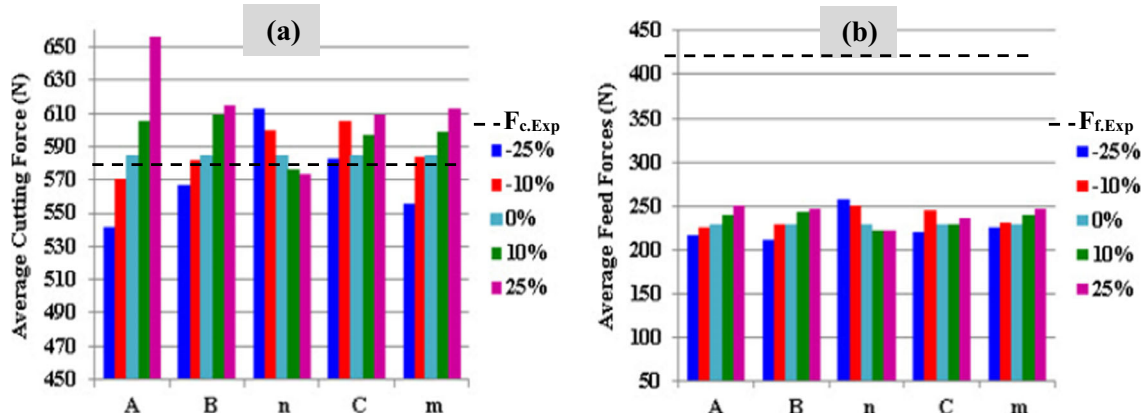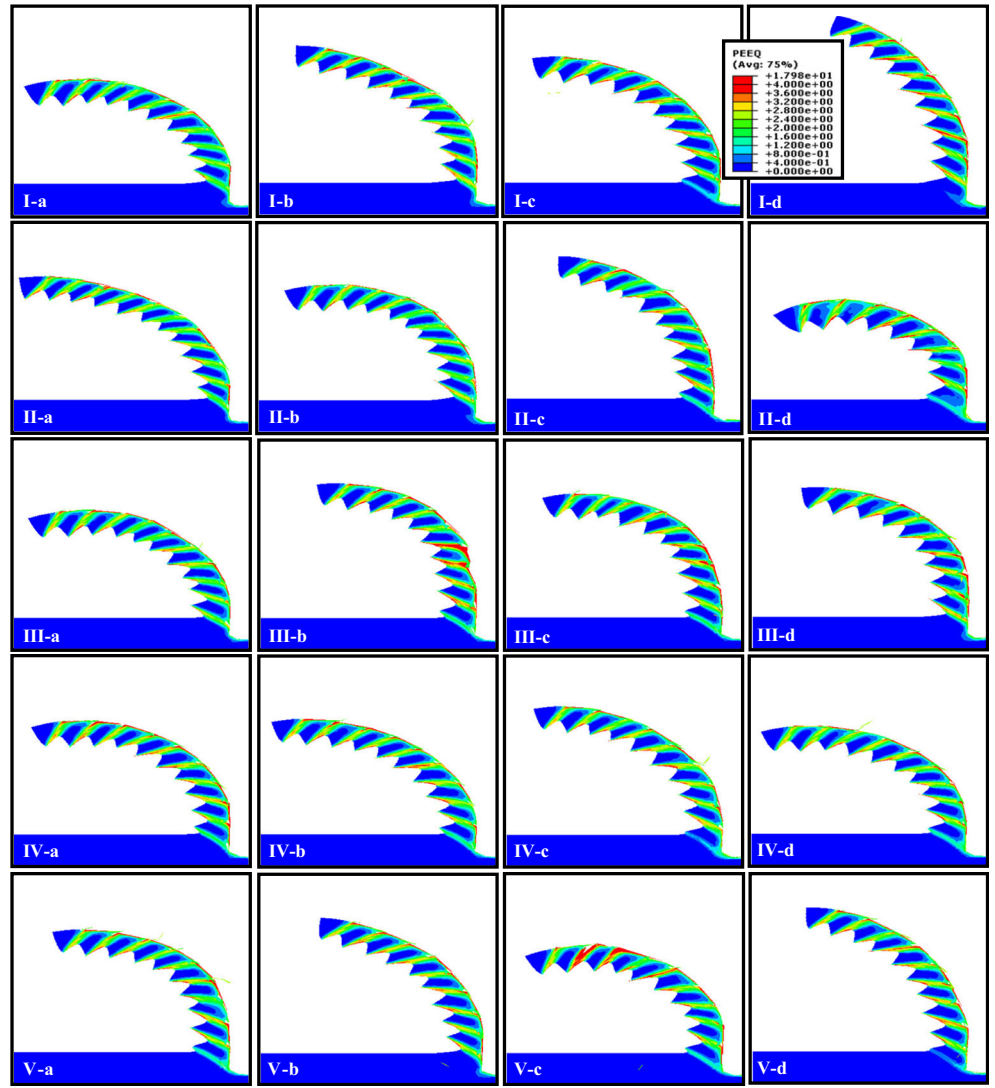


**Fig. 15** Parametric study of the JC plastic model effect on cutting and feed forces ($V_c = 180$ m/min, $a_p = 3$ mm, and $f = 0.1$ mm/rev)

**Fig. 16** Chip serration dependency to JC damage parameters: *I*, *II*, *III*, *IV*, and *V* present respectively *Di* (for i from 1 to 5) while *a*, *b*, *c* and *d* correspond to the range of coefficient variation (−25, −10, +10, and +25 %, respectively)

segmentation has demonstrated a slight change depending on the sense and the percentage of $D_i$ variation. Chip curvature radius $R_c$ has shown in its term its weak sensitivity to JC damage coefficients where no clear trend has been obtained following the increase or the decrease of all the damage initiation model coefficients $D_i$. On the other hand, more curved chip has been noted when more pronounced energy $G_f$ is applied as shown in Fig. 17. Another point to highlight from Fig. 18 is that JC damage definition appears also as of less prominent effect on chip serration sensitivity factor $S_{seg}\%$ compared to $G_f$ which has resulted on pronounced increase in chip serration. $S_{seg}\%$ has been passed from less than −5 %
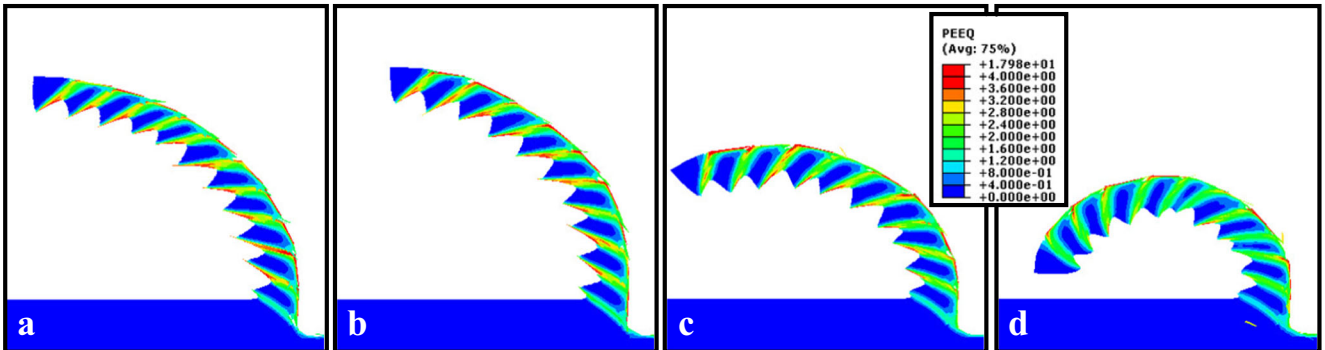


**Fig. 17** Chip morphology dependency to damage evolution definition (**a** −25%$G_{f0}$, **b** −10 % $G_{f0}$, **c** +10 % $G_{f0}$, and **d** +25 % $G_{f0}$)

**Fig. 18** Sensitivity of the chip segmentation factor to damage coefficients definition ($V_c = 75$ m/min, $a_p = 3$ mm, and $f = 0.1$ mm/rev)
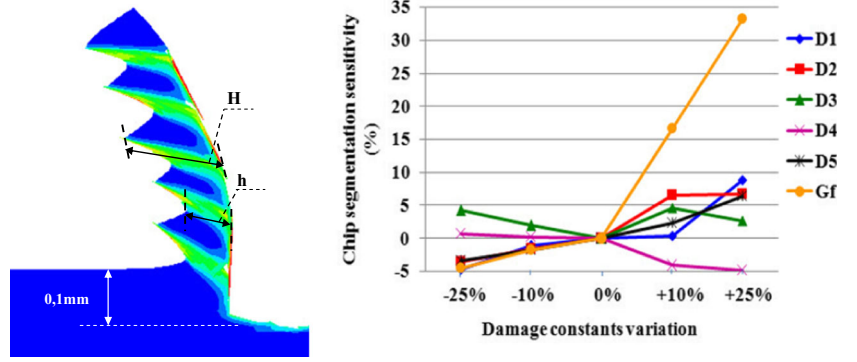
to almost equal to 35 % when damage energy evolution has been increased in a range of 50 % from its initial value $G_{f0}$. However, the maximum variation that has been obtained with the increase of the initial failure strain $D_1$ for example has not exceeded 13 %. This pronounced dependency of the chip segmentation to the accurate definition of damage energy evolution can be attributed to the reduction in the energy required to achieve the total fracture in machined material when $G_f$ is decreased. It is however the accurate implementation of this parameter which greatly counts in regard to the chip serration phenomenon prediction rather than JC damage coefficients definition.

Concerning segmentation frequency $f_{seg}$, the triaxiality exponent factor $D_2$ appears as the most important parameter affecting the aptitude of machined material to accelerate ASBs formation. Additionally, it leads to an increase in the chip saw-teeth number. Examination of the plastic strain evolution along the mid-thickness of the numerical chip obtained with different $D_2$ values has demonstrated a more pronounced delay in $\varepsilon_p$ drop when an overestimation of this failure coefficient has been made as showed in Fig. 19. In fact, an increase in the shear band spacing has been

obtained contributing to larger chip segments and less serration frequency for the same machined surface. However, $\varepsilon_{p(in)}$ and $\varepsilon_{p(out)}$ appear almost insensitive to $D_2$ and even to all JC damage parameters.

Figure 20 illustrates numerical average tangential and feed efforts dependency to damage parameters definition. The same trend has been noted where the failure energy evolution definition has shown the most conspicuous influence on numerical model reliability in terms of cutting forces prediction where a variation about 120 and 70 N in respectively $F_c$ and $F_f$ is obtained with $G_f$ variation. In contradiction with chip morphology, all the coefficients of the JC triaxiality term ($D_1$, $D_2$, and $D_3$) are of interesting effect on the prediction of numerical forces applied whether to the rake or flank cutting tool faces. For example, the increase in triaxiality exponent factor from−25 to +25 % of its initial value has resulted on a rise about 13 and 15 % in tangential and feed forces which is at all negligible especially when high precision of the FE model is focused. In general, the temperature term of the JC damage model has demonstrated the fewest effect on either chip morphology or cutting forces.

**Fig. 19** Dependency of equivalent plastic strain to triaxiality exponent factor $D_2$
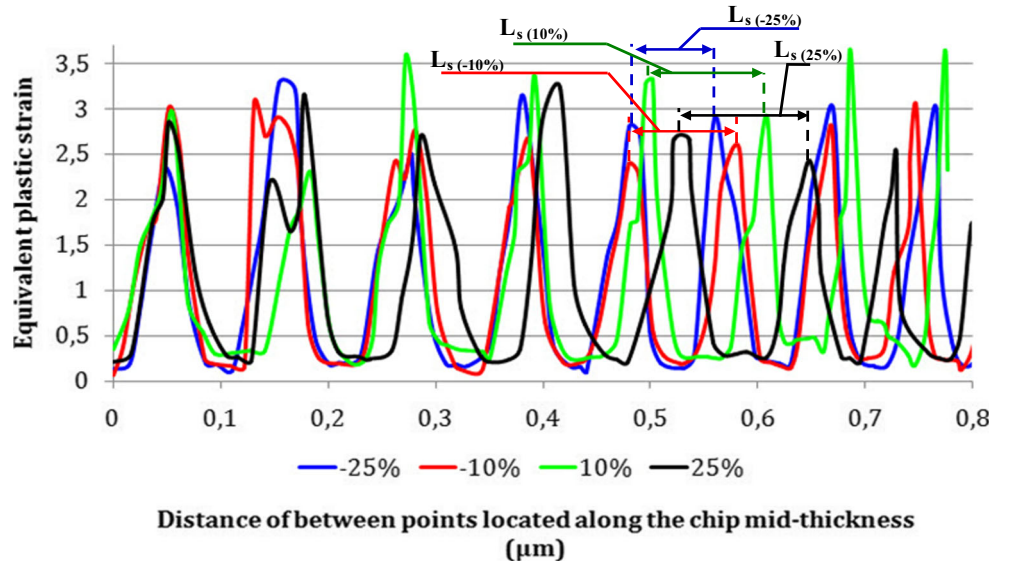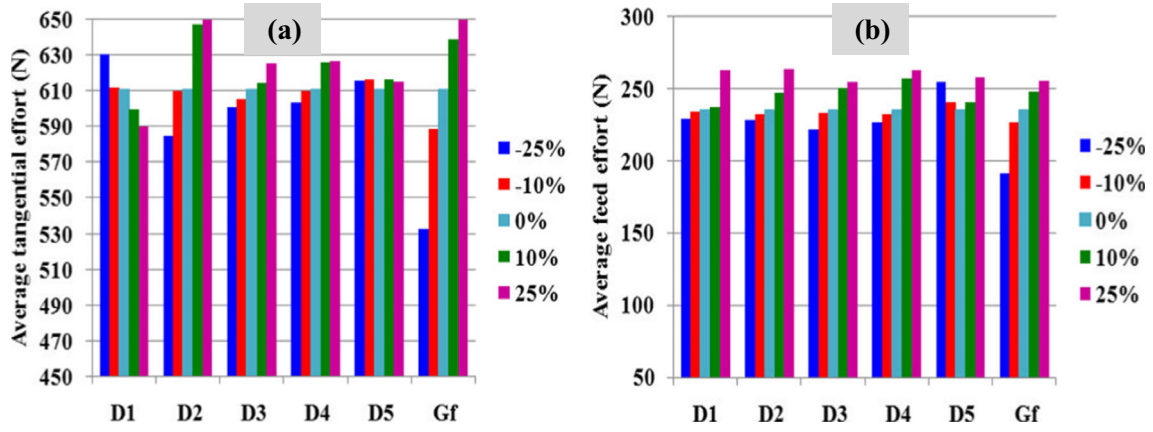
**Fig. 20** Damage parameters effects on cutting forces prediction ($V_c = 75$ m/min, $a_p = 3$ mm, and $f = 0.1$ mm/rev)

## 4 Conclusion

Dependency of Ti6Al4V machining modeling to plastic and damage coefficients definition as well as to cutting speed has been performed in this investigation. A special focus has been attached to the chip serration prediction and its characteristics determination. In addition to segmentation frequency, chip curvature radius, shear band spacing, and cutting forces determination, the serration sensitivity factor, the plastic strain evolution along the mid-thickness of the chip, and the segmentation intensity have been defined and used to quantify the predictability of the FE model and to determine the most affecting constitutive parameters on simulation reliability. Major aim of this paper was to minimize as possible from the miscorrelation between predicted and experimental results while determining with enough precision the main causes of the obtained disagreement. Principal findings of this paper are as follow:

- Chip curvature radius ($R_c$), average peak ($H$), and valley ($h$) chip thickness as well as serration sensitivity factor ($S_{seg}\%$) are quietly affected by the adequate definition of the JC plastic strain hardening term ($A$, $B$, and $n$), the thermal softening parameter ($m$), and the fracture energy evolution ($G_f$) with less (or even no) effect to all the other constitutive coefficients.
- Determination of plastic strain evolution within the chip thickness demonstrates that shear bands spacing ($L_s$) and consequently chip segmentation frequency ($f_{seg}$) are influenced by JC triaxiality exponent parameter ($D_2$) as well as by cutting speed definition. It has been demonstrated that this later additionally affects reached plastic strain levels in and out the formed shear bands and influence on the chip segmentation intensity factor (CSI).
- A well correlation has been established between chip segmentation intensity (CSI) and chip curvature radius ($R_c$) in one hand and cutting forces levels on the other hand where this latter has shown its dependency to the definition of JC

initial yield stress ($A$), its hardening modulus ($B$), its work hardening exponent ($n$), and its thermal softening coefficient ($m$). Additionally, the application of higher cutting speed has resulted on more accentuated change in numerical tangential forces while the decrease in cutting tool velocity has highlighted more pronounced dependency of the average feed forces to JC coefficients.

- Concerning cutting forces dependency to damage definition, initial failure strain ($D_1$), triaxiality factors ($D_2$ and $D_3$), strain rate damage parameter ($D_4$), and failure energy evolution ($G_f$) have exhibited also a non-negligible effect on numerical forces prediction.

Briefly, the usefulness of the present work findings is to give guidance to further numerical cutting modeling accuracy amelioration with minimum efforts when consequences of the wrong definition of specific constitutive model coefficients either on segmented chip geometry or on local plastic strain evolution within or even on cutting forces are previously known.

## References

1. Daoud M, Chatelain JF, Bouzid A (2015) Effect of rake angle on Johnson-Cook material constants and their impact on cutting process parameters of Al2024-T3 alloy machining simulation. Int J Adv Manuf Technol 81:1987–1997
2. Arrazola PJ, Ugate D, J.Montoya, Villar A, Marya S (2005) Finite element modeling of chip formation process with Abaqus/Explicit™6.3. VIII International Conference on Computational Plasticity COMPLAS VIII
3. Sutter G, List G (2013) Very high speed cutting of Ti-6Al-4V titanium alloy-change in morphology and mechanism of chip formation. Int J Mach Tools Manuf 66:37–43
4. Molinari A, Soldani X, Miguélez MH (2013) Adiabatic shear banding and scaling laws in chip formation with application to cutting of Ti-6Al-4V. J Mech Phys Solids 61:2331–2359

5. Ginting A, Nouari M (2009) Surface integrity of dry machined titanium alloys. Int J Mach Tools Manuf 49:325–332

6. Muñez-Sánchez A, Canteli JA, Cantero JL, Miguélez MH (2011) Numerical analysis of the tool wear effect in the machining induced residual stresses. Simul Model Pract Theory 19:872–886

7. Davies MA, Chou Y, Evans CJ (1996) On chip morphology, tool wear and cutting mechanics in finish hard turning. CIRP Ann Manuf Technol 45:77–82

8. Molinari A, Musquar C, Sutter G (2002) Adiabatic shear banding in high speed machining of Ti-6Al-4V: experiments and modeling. Int J Plast 18:443–459

9. Calamaz M, Coupard D, Girot F (2008) A new material model for 2D numerical simulation of serrated chip formation when machining titanium alloy Ti-6Al-4V. Int J Mach Tools Manuf 48:275–288

10. Wang B, Lui Z, Yang Q (2013) Investigations of the yield stress, fracture toughness and energy distribution in high speed orthogonal cutting. Int J Mach Tools Manuf 73:1–8

11. Komanduri R, Von Turkovich BF (1981) New observations on the mechanism of chip formation when machining titanium alloys. Wear 69:179–188

12. Ambati R, Yuan H (2011) FEM mesh-dependence in cutting process simulations. Int J Adv Manuf Technol 53:313–323

13. Hua J, Shivpuri R (2004) Prediction of chip morphology and segmentation during the machining of titanium alloys. J Mater Process Technol 150:124–133

14. Shaw MC, Vyas A (1998) The mechanism of chip formation with hard turning steel. CIRP Ann Manuf Technol 47:77–82

15. Lin ZC, Lin YY (2001) Three dimensional elastic-plastic finite element analysis for orthogonal cutting with discontinuous chip of 6-4 brass. Theor Appl Fract Mech 35:137–153

16. Deshayes L, Mabrouki T, Ivester R, Rigal JF (2004) Serrated chip morphology and comparison with finite element simulations. Proceedings of IMECE2004-ASME 2004 International Mechanical Engineering Congress and Exposition

17. Ducobu F (2013) Contribution à l'étude de la formation du copeau de Ti6Al4Ven coupe orthogonale-Approches numérique et expérimentale pour la compréhension des mécanismes de coupe macroscopique et microscopique. PhD Thesis, Polytechnic Faculty of Mons, Belgium

18. Braham-Bouchnak T (2010) Etude du comportement en sollicitations extrêmes et de l'usinabilité d'un nouvel alliage de titane aéronautique: le Ti555-3. PhD Thesis, Centre of Angers, France

19. Sartkulvanich P, Altan T, Soehner J (2005) Flow stress data for finite element simulation in metal cutting: a progress report on madams. Mach Sci Technol 9:271–288

20. Chen G, Ren C, Yang X, Jin X, Guo T (2011) Finite element simulation of high-speed machining of titanium alloy (Ti-6Al-4V) based on ductile failure model. Int J Adv Manuf Technol 56:1027–1038

21. Germain G, Morel A, Braham-Bouchnak T (2013) Identification of material constitutive laws representative of machining conditions of two titanium alloys: Ti6Al4V and Ti555-3. J Eng Mater-T ASME 135

22. Daoud M, Jomoaa W, Chatelain JF, Bouzid A (2015) A machining-based methodology to identify material constitutive law for finite element simulation. Int J Adv Manuf Technol 77:2019–2033

23. Agmell M, Ahadi A, Ståhl J-E (2013) The link between plasticity parameters and process parameters in orthogonal cutting. 14th CIRP Conference on Modelling of Machining Operations 8:224–229

24. Umbrello D, M'Saoubi R, Outeiro JC (2007) The influence of Johnson-Cook material constants on finite element simulation of machining of AISI 316L steel. Int J Mach Tools Manuf 47:462–470

25. Guo YB, Wen Q, Woodbury KA (2006) Dynamic material behavior modeling using internal state variable plasticity and its application in hard machining simulations. J Manuf Sci Eng 128:749–756

26. Ducobu F, Rivière-Lorphèvre E, Filippi E (2014) Numerical contribution to the comprehension of saw-toothed Ti6Al4V chip formation in orthogonal cutting. Int J Mech Sci 81:77–87

27. Calamaz M (2008) Approches expérimentale et numérique de l'usinage à sec de l'alliage aéronautique TA 6V. PhD Thesis, University of Bordeaux, France

28. Barge M, Hamdi H, Rech J, Bergheau J-M (2005) Numerical modelling of orthogonal cutting: influence of numerical parameters. J Mater Process Technol 164–165:1148–1153

29. Johnson GR, Cook WH (1983) A constitutive model and data for metals subjected to large strains, high strain rates and high temperatures. Proceedings of the Seventh International Symposium on Ballastics, The Hague, the Netherlands, 541-547

30. Mabrouki T, Girardin F, Asad M, Rigal J-F (2008) Numerical and experimental study of dry cutting for an aeronautic aluminum alloy. Int J Mach Tools Manuf 48:1187–1197

31. Umbrello D (2008) Finite element simulation of conventional and high speed machining of Ti6Al4V alloy. J Mater Process Technol 196:79–87

32. Guo YB, Yen DW (2004) A FEM study on mechanisms of discontinuous chip formation in hard machining. J Mater Process Technol 155–156:1350–1356

33. Sima M, Özel T (2010) Modified material constitutive models for serrated chip formation simulations and experimental validation in machining of titanium alloy Ti-6AL-4V. Int J Mach Tools Manuf 50:943–960

34. Calamaz M, Coupard D, Nouari M, Girot F (2011) Numerical analysis of chip formation and shear localisation processes in machining the Ti-6Al-4V titanium alloy. Int J Adv Manuf Technol 52:887–895

35. Ohbuchi Y, Obikawa T (2005) Adiabatic shear in chip formation with negative rake angle. Int J Mech Sci 47:1377–1392

36. Rhim S-H, Oh S-I (2006) Prediction of serrated chip formation in metal cutting process with new flow stress model for AISI 1045 steel. J Mater Process Technol 171:417–422

37. Johnson GR, Cook WH (1985) Fracture characteristics of three metals subjected to various strains, strain rates, temperatures and pressures. Eng Fract Mech 21:31–48

38. Hillerborg A, Modéer M, Petersson P-E (1976) Analysis of crack formation and crack growth in concrete by means of fracture mechanics and finite elements. Cem Concr Res 6:773–782

39. Zhang Y, Outeiro JC, Mabrouki T (2015) On the selection of Johnson-Cook constitutive model parameters for Ti-6Al-4V using three types of numerical models of orthogonal cutting. 15th CIRP Conference on Modelling of Machining Operations 31:112-117

40. ABAQUS User's Manual (2013) Abaqus/Explicit® version 6.13. Dassault Systems Simulia Corp., Providence

41. Liu J, Bai Y, Xu C (2013) Evaluation of ductile fracture models in finite element simulation of metal cutting processes. Journal of Manufacturing Science Engineering 136(1)

42. Miguelez MH, Soldani X, Molinari A (2013) Analysis of adiabatic shear banding in orthogonal cutting of Ti alloy. Int J Mech Sci 75:212–222

43. Haddag B, Abed-Meraim F, Balan T (2009) Strain localization analysis using a large deformation anisotropic elastic-plastic model coupled with damage. Int J Plast 25:1970–1996

44. Shet C, Deng X (2000) Finite element analysis of the orthogonal metal cutting process. J Mater Process Technol 105:95–109

45. Özel T (2006) The influence of friction models on finite element simulations of machining. Int J Mach Tools Manuf 46: 518–530

46. Filice L, Micari F, Rizzuti S, Umbrello D (2007) A critical analysis on the friction modelling in orthogonal machining. Int J Mach Tools Manuf 47:709–714

47. Zorev NN (1963) Inter-relationship between shear processes occurring along the tool face and shear plane in metal cutting. International Research in Production Engineering ASME 42-49

48. Atlati S, Haddag B, Nouari M, Zenasni M (2011) Analysis of a new segmentation intensity ratio "SIR" to characterize the chip segmentation process in machining ductile metals. Int J Mach Tools Manuf 51:687–700

49. Haddag B, Atlati S, Nouari M, Znasni M (2010) Finite element formulation effect in three-dimensional modeling of a chip formation during machining. Int J Mater Form 3:527–530

50. Sun S, Brandt M, Dargusch MS (2009) Characteristics of cutting forces and chip formation in machining of titanium alloys. Int J Mach Tools Manuf 49:561–568

51. Wang B, Liu Z (2015) Shear localization sensitivity analysis for Johnson-Cook constitutive parameters on serrated chips in high speed machining of Ti6Al4V. Simul Model Pract Theory 55:63–76